GEOPHYSICS, VOL. 73, NO. 3 (MAY-JUNE 2008); P. S99–S114, 10 FIGS., 2 TABLES.
10.1190/1.2907736

Image-ray tracing for joint 3D seismic velocity estimation and time-to-depth conversion

Einar Iversen[1] and Martin Tygel[2]

ABSTRACT

Seismic time migration is known for its ability to generate well-focused and interpretable images, based on a velocity field specified in the time domain. A fundamental requirement of this time-migration velocity field is that lateral variations are small. In the case of 3D time migration for symmetric elementary waves (e.g., primary PP reflections/diffractions, for which the incident and departing elementary waves at the reflection/diffraction point are pressure [P] waves), the time-migration velocity is a function depending on four variables: three coordinates specifying a trace point location in the time-migration domain and one angle, the so-called migration azimuth. Based on a time-migration velocity field available for a single azimuth, we have developed a method providing an image-ray transformation between the time-migration domain and the depth domain. The transformation is obtained by a process in which image rays and isotropic depth-domain velocity parameters for their propagation are estimated simultaneously. The depth-domain velocity field and image-ray transformation generated by the process have useful applications. The estimated velocity field can be used, for example, as an initial macrovelocity model for depth migration and tomographic inversion. The image-ray transformation provides a basis for time-to-depth conversion of a complete time-migrated seismic data set or horizons interpreted in the time-migration domain. This time-to-depth conversion can be performed without the need of an a priori known velocity model in the depth domain. Our approach has similarities as well as differences compared with a recently published method based on knowledge of time-migration velocity fields for at least three migration azimuths. We show that it is sufficient, as a minimum, to give as input a time-migration velocity field for one azimuth only. A practical consequence of this simplified input is that the image-ray transformation and its corresponding depth-domain velocity field can be generated more easily.

INTRODUCTION

Time migration (prestack or poststack) is a well-established and routinely applied procedure to obtain time-domain images from seismic reflection data. For simple velocity models, time migration is characterized by its ability to obtain focused images in the time domain. Depth migration, on the other hand, can produce focused structural images in the depth domain for complex velocity variations. The main advantage of the time-migration procedure is that it produces fairly interpretable images quickly and inexpensively. Except for strong lateral velocity variations, time migration is very robust with respect to inaccuracies of the time-domain velocity model. This is to be compared with the much more involved depth migration, especially prestack, which requires, besides a well-designed depth-domain velocity model, significantly more computational effort.

As compared with common-midpoint (CMP) stacking, which essentially produces seismic data sets corresponding to a simulated zero-offset (ZO) acquisition, the time migration process generates data sets with features that are identified more easily with structures in the depth domain. In particular, triplications typical for unmigrated images of synclinal structures naturally unfold to synclinals after time migration.

For any time-domain imaging procedure, the image of a reflector is called a reflecting horizon. For the same reflector in the depth domain, the overall characteristics, kinematic and dynamic, of its corresponding reflecting horizon will depend strongly on the acquisition configuration and imaging procedure that is employed. In accordance with the ray methods that will be used throughout, we envis-

Manuscript received by the Editor 14 December 2006; revised manuscript received 14 November 2007; published online 7 May 2008.
[1]NORSAR, Kjeller, Norway. E-mail: einar.iversen@norsar.com.
[2]State University of Campinas (UNICAMP), Applied Mathematics Department, IMECC, Campinas, Brazil. E-mail: mtygel@gmail.com.

age the reflector as a smooth continuum of independent point scatterers (or point diffractors) which, because of illumination by seismic waves, are excited and emit energy toward the surface. Under this formulation, the image of a reflector can be understood as the ensemble of the individual (time-domain) images of the point scatterers that constitute the (depth-domain) reflector. A review of basic formulas constituting the 3D Kirchhoff prestack time-migration procedure is given in Appendix A.

The basic goal of time migration is to focus the seismic energy into interpretable time-domain images. Concerning accuracy, especially with respect to reflector positioning, quite a long struggle exists in the literature on the pros and cons of prestack and poststack time migration. As a rule, the widespread use of time migration is a testimony of its practical usefulness (see, for example, Yilmaz, 2001). Sound criticism of time migration, both in theoretical and practical aspects, can be found in, for example, Black and Brzostowski (1994), Whitcombe (1994) and, more recently, Robein (2003, Chapter 8).

The time-migration process is quite robust with respect to perturbations of the time-migration velocity model. However, because time migration commonly is based on a hyperbolic traveltime approximation, its applicability is limited to velocity models with small lateral variations (Yilmaz, 2001). Historically speaking, "ideal" or "complete" time migration has been considered a process positioning the reflecting horizons "vertically above" their corresponding reflectors in the depth domain. More specifically, the horizontal coordinates of each point scatterer on a reflector then would coincide with the horizontal coordinates (trace location) of its associated time-migrated image. For this idealized process, it is assumed that the connection between each point scatterer at the reflector and its trace location at the surface can be realized by a vertical ray. As a consequence, the transformation of the traveltime coordinate of a point on a time-migrated reflecting horizon to the depth coordinate of its associated point scatterer at the reflector (the so-called time-to-depth conversion) would be achieved by a simple scaling operation, namely, multiplication of half the traveltime by an appropriate (average) medium velocity along the vertical ray.

The above concept of a complete time migration, although useful as a theoretical framework, is not realistically possible. As explained in Hubral (1977), the closest feasible alternative is to have a transformation that uses image rays (and not vertical rays) to connect the point scatterers at the reflector to their corresponding trace locations at the surface. For an arbitrary point scatterer on the reflector, the *image ray* can be defined as a ray connecting the scatterer to the measurement surface in such a way that the slowness vector is normal to that surface. This definition allows the medium below the measurement surface to be either isotropic or anisotropic. Likewise, the *normal ray* can be defined as a ray connecting the point scatterer to the measurement surface in such a way that the slowness vector is normal to the reflector (Iversen, 2006). As also described in Hubral (1977), assuming an isotropic velocity model, the following duality exists for normal rays and image rays that connect surface measurement to a given reflector scatterer. The former is normal to the reflector, whereas the latter is normal to the measurement surface.

In spite of widespread use in seismic processing, time migration also encounters criticism and concern about its application. Black and Brzostowski (1994) report mispositions of events even with correct velocity and propose a general correction scheme, called remedial migration. Whitcombe (1994) pointed out that although time migration produces useful, better interpretable images of reflectors, the time-migrated section is not the best option for subsequent depth conversion. He proposes instead to demigrate the interpreted time-migrated horizons into the unmigrated domain and use normal rays for depth conversion. According to Whitcombe (1994), the method combines the good interpretable properties of time migration with the better positioning provided by depth migration.

From the very definition of time migration, the most consistent depth conversion would be along image rays in such a way that the depth velocities needed for the image-ray tracing would be obtained directly from the given time-migration velocity field. A method that does exactly that was presented recently by Cameron et al. (2006, 2007). Besides time-migrated data, the method requires in its 3D version that the time-migrated velocity field is available for at least three directions along the measurement surface. This requirement might impose some limitations to the applications of the method in practice.

Our objective is to present theory and numerical examples for a 3D image-ray tracing and velocity-estimation algorithm in which it is sufficient to know the time-migration velocity field in a single direction only. Our approach is similar to that of Cameron et al. (2006, 2007), but the range of practical applications is extended. A discussion on the actual differences between the two approaches is provided in Appendix B.

NOMENCLATURE

To make the mathematical derivations easier to follow, lists of the most important symbols used in the text are displayed in Table 1. Lowercase and uppercase letters i and I used as subscripts can have the values $i = 1,2,3$, and $I = 1,2$, respectively. For three-component vectors, we use standard notation, for example, $\mathbf{a}$, whereas for two-component vectors, a bar is printed above the symbol, as in $\bar{\mathbf{a}}$. Vectors are considered equivalently as column matrices. To distinguish between matrices of size 3×3 and 2×2, we use notations $\hat{\mathbf{A}}$ and $\mathbf{A}$, respectively. The notation $\mathbf{A}^T$ is used for the transpose of the matrix $\mathbf{A}$, and $\mathbf{A}^{-T}$ is a shorthand notation for $\mathbf{A}^{-1^T}$. For cases in which ambiguity can arise, a superscript in the form (q) on vectors/matrices serves as a label for the coordinate system under consideration. The 3×1 column vector containing the first partial derivatives and the 3×3 matrix containing the second partial derivatives of a scalar field W with respect to the variables, $\mathbf{x} = (x_i)$, are written in the forms

$$\frac{\partial W}{\partial \mathbf{x}} = \left(\frac{\partial W}{\partial x_i}\right) \quad \text{and} \quad \frac{\partial^2 W}{\partial \mathbf{x}^2} = \left(\frac{\partial^2 W}{\partial x_i \partial x_j}\right). \tag{1}$$

KIRCHHOFF TIME AND DEPTH MIGRATION

In the following, we review the basics of Kirchhoff time and depth migration as needed in this article.

Depth migration

A good understanding of how time migration can be carried out can be gained by examining its relationship to Kirchhoff depth migration, as applied to a single stacked section. Such a procedure is referred to as 2D Kirchhoff poststack depth migration. For a given depth-domain macrovelocity model and a given point in the depth domain D to be imaged, the Kirchhoff depth-migration operation ba-

sically consists of a weighted sum of data samples along the diffraction time surface associated with D, the result of that sum being assigned at D.

Under the assumption that a stacked section well approximates (or simulates) a ZO section, the diffraction time surface associated with the fixed point D is given by the two-way times along the rays that connect D to the varying coincident (ZO) source-receiver points at the measurement surface. According to the theory of Kirchhoff migration (see, for example, Tygel et al., 1996), for a sufficiently accurate macrovelocity model, the summing operation along the diffraction time surface associated with a point at a reflector will be approximately tangent to its corresponding reflecting horizon in the stacked section. As a consequence, the Kirchhoff summation will provide significant values at the image points D which lie at or are very close to a reflector. For image points D away from reflectors, the corresponding summation will yield negligible values. The migrated depth-domain section is obtained by applying the Kirchhoff summation to a previously defined densely sampled collection of image points D (e.g., a regular grid).

The above considerations show that the Kirchhoff process establishes for any individual depth reflector a correspondence (or mapping) between each point scatterer on the reflector and the tangency point where the diffraction traveltime surface associated with the point scatterer meets the reflecting horizon in the stacked section. Hubral (1977) refers to these tangency points as "scattering centers for seismic waves." The Kirchhoff migration thus associates each scatterer on the reflector to its corresponding scattering center at the reflecting horizon. Finally, we observe that any point scatterer on the reflector is connected to the projection on the measurement surface of its corresponding scattering center by the normal ray.

For an isotropic depth-velocity model with horizontal interfaces and no lateral velocity variations, it is clear that for each point scatterer on a reflector, the normal and image rays coincide, both being vertical. In this case, the stacked section also coincides with the time-migrated section, and that also represents a "complete" time migration, which corresponds to vertical image rays. Apart from this extremely simple situation, stacking and time migration are bound to yield very different images of the same depth model.

Table 1. The most important symbols used in the text.

Symbol	Meaning
$\mathbf{x} = (x_i)$	Global Cartesian coordinates of the depth domain
$\bar{\mathbf{s}}$, $\bar{\mathbf{r}}$, $\bar{\mathbf{x}} = (\bar{\mathbf{s}} + \bar{\mathbf{r}})/2$, $\bar{\mathbf{y}} = (\bar{\mathbf{s}} - \bar{\mathbf{r}})/2$	Source/receiver and midpoint/half-offset coordinates at measurement surface
$\bar{\mathbf{x}}^M$, $\bar{\mathbf{a}} = \bar{\mathbf{x}} - \bar{\mathbf{x}}^M$	Time-migration apex and aperture vectors at measurement surface
t	Time variable of the unmigrated time domain
t^M	Time variable of the migrated time domain
$(\bar{\mathbf{x}},t)$	Unmigrated time-domain coordinates
$(\bar{\mathbf{x}}^M,t^M)$	Migrated time-domain coordinates
θ	Migration azimuth
$\bar{\mathbf{u}} = (\cos\theta, \sin\theta)^T$	Unit vector in the migration azimuth direction
$\boldsymbol{\gamma} = (\gamma_i)$, $\gamma_I = x_I^M$, $\gamma_3 = T = t^M/2$	Ray coordinates for a field of image rays
$\mathbf{q} = (q_i)$	Local Cartesian coordinates along the image ray
$(\bar{\mathbf{q}}, \gamma_3)$, $\gamma_3 = T$	Ray-centered coordinates along the image ray
$v^M(\bar{\mathbf{x}}^M,t^M)$	Time-migration velocity field for a given migration azimuth
$v^M_{\text{dix}}(\hat{\boldsymbol{\gamma}})$	Time-migration interval velocity field for a given migration azimuth
$v(\mathbf{x})$, $v(\mathbf{q})$	Depth-domain velocity field in global and local Cartesian coordinates
$v(\boldsymbol{\gamma})$	Depth-domain velocity field in ray coordinates
$F(\boldsymbol{\gamma})$	Velocity spreading factor
$\hat{\mathbf{M}}^{(x)}$	3×3 symmetric matrix corresponding to azimuth-dependent migration velocity
$\mathbf{x}$, $\mathbf{p}$	Position and slowness vectors of image rays
$\mathbf{x}^0$, $\mathbf{p}^0$, v^0, $\mathbf{e}_1^0$, $\boldsymbol{\Pi}^0$, and $\boldsymbol{\gamma}^0$	Image-ray quantities at the initial point $\boldsymbol{\gamma}^0 = (x_I^{M0}, t^{M0} = 0)$
$\hat{Q}_1^{(x)}$, $\hat{\mathbf{Q}}_1^{(q)}$	3×3 matrices $(\partial x_i/\partial\gamma_j)$ and $(\partial q_i/\partial\gamma_j)$ in global and local Cartesian coordinates, corresponding to plane-wave initial condition
$\boldsymbol{\Pi}$	Ray-propagator matrix
$\mathbf{Q}_1$, $\mathbf{P}_1$	First set of paraxial matrices, corresponding to plane-wave initial condition
$\mathbf{Q}_2$, $\mathbf{P}_2$	Second set of paraxial matrices, corresponding to point-source initial condition
$\mathbf{H} = (\mathbf{e}_1\ \mathbf{e}_2\ \mathbf{e}_3)$	3×3 transformation matrix with columns $\mathbf{e}_i$, the ith unit vector of the local Cartesian coordinate system along the image ray

Time migration

Time migration can be carried out by a simple modification to the above-described Kirchhoff poststack depth migration. After stacking along the diffraction traveltime surface of a given depth point D, all we need to do is to assign the stacking result (the migration output) to the apex of the diffraction traveltime surface instead of assigning it to the original depth point D, as would be done in the Kirchhoff depth-migration counterpart. A geometric outline of the procedure is depicted in Figure 1. The reasoning for the approach is simple: The apex of the diffraction traveltime surface for a point scatterer D represents the stationary traveltime from that point to the measurement surface. As a consequence, the image ray from D is the one that has that stationary traveltime.

An underlying assumption of the procedure is that the diffraction traveltime surface is sufficiently well behaved so that a clear apex exists. In the absence of abrupt lateral velocity variations, each diffraction traveltime surface can be approximated well by a hyperboloid in the vicinity of its apex. It is then possible to formulate a time-migration procedure that is based on time-domain computations only, so that dependency on a depth-domain macrovelocity can be avoided. Consider for simplicity a single unmigrated zero-offset section where the inline coordinate is x and the two-way time is t. For each given point (x^M,t^M) in the time-migrated section to be constructed, introduce the hyperbolic traveltime function,

$$[t^D(x)]^2 = (t^M)^2 + \frac{4}{(v^M)^2}(x - x^M)^2, \qquad (2)$$

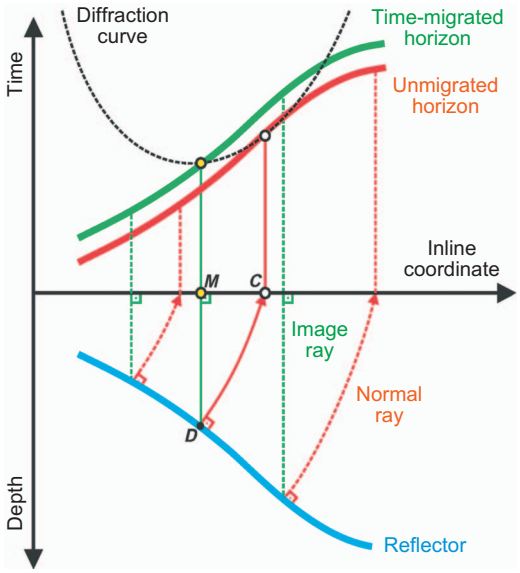

Figure 1. Geometric outline of time-migration procedure in the simple 2D poststack situation. A diffraction point D on a reflector (blue) in the depth domain is connected by a normal ray (solid red) to a common midpoint C on the measurement surface. An image ray (solid green) connects point D to the projected apex point M belonging to a diffraction curve (dashed black), which is tangent to the unmigrated horizon (the time-domain counterpart of the reflector, shown in red) at point C. The time-migrated horizon (green) represents the continuum of all diffraction-curve apexes related in this way to the unmigrated horizon.

along which seismic data for the samples (x,t) in the given unmigrated zero-offset section are stacked. The quantity $v^M = v^M(x^M,t^M)$ in equation 2 is the time-migration velocity or, in short, the migration velocity. We remark that equation 2 is relevant for 2D poststack time migration only and is included here only to introduce briefly the underlying philosophy behind the time-migration concept. For a description of a corresponding equation that governs 3D prestack time migration, the reader is referred to Appendix A.

A basis for any Kirchhoff time-migration procedure (2D/3D/poststack/prestack) is the knowledge of a migration velocity field. Let us emphasize that an in-depth description of the various methods to perform time migration and migration-velocity analysis is outside the scope of the present paper. For that, the reader is referred to, for example, Yilmaz (2001). Here, we only briefly indicate how the migration velocity can be obtained. One common option in the past was to use the stacking (NMO) velocity that previously had been determined for obtaining the CMP-stacked section and eventually apply an ad hoc scaling factor to it. For dipping structures, an approach often considered as more adequate has been to use as migration velocity an NMO velocity corrected for dip moveout (DMO); see Hale (1984). An example of a modern, automated migration-velocity estimation scheme is reported in Fomel (2003). A discussion on recent approaches of time-migration velocity analysis and their use in practical applications is given in Robein (2003).

TIME-TO-DEPTH CONVERSION

The final aim of kinematic seismic imaging is to position reflectors correctly in the depth domain. In this way, time-domain images such as CMP-stacked or time-migrated sections represent intermediate, although very useful, results. A subsequent operation that transforms a time-domain seismic data set into its corresponding depth-domain data set is referred to as time-to-depth conversion.

Assume for simplicity that the measurement surface is a horizontal plane located at zero depth. In an analogy to previous notation, let the unmigrated data set be described by the coordinates (x_1,x_2,t), where the first two coordinates, x_1 and x_2, specify the location of the CMP on the measurement surface, and the third coordinate t is time. Time-to-depth conversion of an unmigrated data set requires that normal rays can be traced from the measurement surface. This is possible if information from the time-domain data set as well as adequate structural assumptions for the subsurface allows one to derive a suitable depth-domain velocity model and the initial directions and two-way times of the normal rays. In this situation, an event located in the point (x_1,x_2,t) of the unmigrated data set is converted from time to depth by constructing the normal ray that starts at the common midpoint $(x_1,x_2,x_3 = 0)$ and proceeds to its end point, determined by the criterion that half of the given two-way time of the event $t/2$ is consumed.

Under the assumption of a 3D isovelocity layered model with smoothly curved interfaces, Hubral and Krey (1980) propose a recursive algorithm to recover the layer velocities, as well as the positions and curvatures of the interfaces, from knowledge of the traveltime function and the first two derivatives with respect to the coincident source-receiver horizontal location of each reflecting horizon in the unmigrated data set. Geometrically, the first derivatives of traveltime are related to the direction of incidence of the normal ray in the emergence point on the measurement surface. The second derivatives are related to the radii of curvature of the so-called normal-incidence point (NIP) wave in this emergence point.

In a manner analogous to the previous considerations, time-to-depth conversion of time-migrated seismic data will be possible if the information in the time-domain data allows one to trace image rays in the depth domain. An advantage of such a process, compared with the previous case involving the unmigrated data set, is that image rays have a known initial condition, namely, that the initial slowness vector is perpendicular to the measurement surface. For each point (x_1^M, x_2^M, t^M) in the time-migration domain, the time-to-depth conversion moves the event at this point along the image ray that starts at $(x_1 = x_1^M, x_2 = x_2^M, x_3 = 0)$ on the measurement surface and proceeds into the depth domain until half of the given time, $t^M/2$, is consumed. For a 3D isovelocity layered macrovelocity model in the depth domain, Hubral and Krey (1980) describe an algorithm to transform along image rays the locations, dips, and curvatures for horizon points in the time-migration domain to corresponding locations, dips, and curvatures for horizon points in the depth domain. A generalization of this algorithm to include heterogeneous layers is described by Iversen et al. (1987, 1988).

THEORY

In this section, we explain how we can trace image rays into depth and simultaneously estimate the velocity along them from knowledge of a 3D time-migration velocity field in an arbitrary single direction along the measurement surface. We observe that the required single-direction velocities are extracted from an underlying full 3D time-migration velocity field.

Coordinate systems

The construction of image rays, as envisaged by our methodology, relies mainly on the concepts and results of standard kinematic and dynamic ray tracing, as described, for example, in Červený (2001). In this way, it is instrumental to introduce, besides a global depth-domain Cartesian coordinate system, $\mathbf{x} = (x_i)$, additional coordinate systems that will be associated with the image rays.

The first of these to be mentioned here is the coordinate system associated with the time-migration domain, (x_1^M, x_2^M, t^M). Closely connected to the latter is the ray coordinate system $\boldsymbol{\gamma} = (\gamma_i)$, which defines the image rays issued from all trace locations of the time-migrated seismic data set. This means that the first two coordinates are defined as $\gamma_1 = x_1^M$ and $\gamma_2 = x_2^M$. For the variable along the ray γ_3, we shall use the one-way traveltime, denoted by the symbol T. In other words, we have $\gamma_3 = T = t^M/2$. The 3D curvilinear space formed by the ray coordinates is referred to as the ray domain. Finally, we shall need also the ray-centered coordinate system, (q_1, q_2, γ_3), introduced by Popov and Pšenčík (1978), and a corresponding local Cartesian coordinate system, $\mathbf{q} = (q_i)$, which is attached to each individual point on the image ray. The vectorial function $\mathbf{x}(\boldsymbol{\gamma})$ describes a mapping of a point $\boldsymbol{\gamma}$ in the ray coordinate system onto a point $\mathbf{x}$ in the global Cartesian coordinate system. Because this mapping is based on construction of image rays, we refer to it as image-ray transformation.

Input data

For the combined image-ray tracing and depth-domain velocity estimation, we assume the knowledge of a single-direction time-migration velocity function, $v^M = v^M(\bar{\mathbf{x}}^M, t^M, \theta)$, extracted from a full 3D time-migration velocity field. Here, $\bar{\mathbf{x}}^M = (x_1^M, x_2^M)^T$ specifies a trace in the time-migrated data set, t^M denotes the two-way migration time, and θ is the angle specifying the direction along which the migration velocity is given. This angle is referred to in the following as the migration azimuth or, in brief, azimuth.

Prior to applying our ray-tracing method, it is practical to convert the time-migration velocity by Dix's method to the so-called time-migration interval velocity,

$$v_{\mathrm{dix}}^M(\boldsymbol{\gamma}) = \left\{ \frac{d}{dt^M}[t^M (v^M)^2] \right\}^{1/2} = \left\{ \frac{d}{dT}[T (v^M)^2] \right\}^{1/2}. \quad (3)$$

The function v_{dix}^M must possess only weak variations with respect to the lateral coordinates γ_1 and γ_2. In addition, it is essential for the stability of the ray-tracing procedure that v_{dix}^M and its derivatives $\partial v_{\mathrm{dix}}^M / \partial \gamma_i$ and $\partial^2 v_{\mathrm{dix}}^M / (\partial \gamma_i \partial \gamma_j)$ are smooth functions of all three coordinates γ_i.

Kinematic ray tracing

A basis for kinematic ray tracing in 3D isotropic elastic media can be formulated by the ordinary differential equations (see, for example, Červený, 2001, section 3.1.1)

$$\frac{d\mathbf{x}}{dT} = v^2(\mathbf{x})\mathbf{p},$$
$$\frac{d\mathbf{p}}{dT} = -v^{-1}(\mathbf{x})\frac{\partial v}{\partial \mathbf{x}}. \quad (4)$$

Evaluation of the above kinematic ray-tracing equations requires knowledge of the velocity, $v(\mathbf{x})$, and its gradient, $\partial v/\partial \mathbf{x}$, which we do not have direct access to. As shown below, however, we will overcome this by further analysis that involves the dynamic ray-tracing system.

Dynamic ray tracing

The dynamic ray-tracing system, in 3D isotropic elastic media, now is formulated in ray-centered coordinates. For a fixed image ray, we consider the attached local Cartesian coordinate system $\mathbf{q}$. For each coordinate q_i, we associate a corresponding unit basis vector $\mathbf{e}_i$. These unit vectors constitute the columns of an orthonormal transformation matrix

$$\hat{\mathbf{H}} = (\mathbf{e}_1\ \mathbf{e}_2\ \mathbf{e}_3). \quad (5)$$

The matrix $\hat{\mathbf{H}}$ can be computed in any point along the ray if we include within the system of ray differential equations the following equation

$$\frac{d\mathbf{e}_1}{dT} = -v^2 \left(\mathbf{e}_1 \cdot \frac{d\mathbf{p}}{dT} \right) \mathbf{p}, \quad (6)$$

where $d\mathbf{p}/dT$ is given by the second relation in equation 4. Knowing the vector $\mathbf{e}_3 = \mathbf{p}/\|\mathbf{p}\|$ and the vector $\mathbf{e}_1$ resulting from numerical integration including equation 6, the vector $\mathbf{e}_2$ is obtained easily by the cross product

$$\mathbf{e}_2 = \mathbf{e}_3 \times \mathbf{e}_1. \quad (7)$$

In the following, we use the standard formulation of complete dynamic ray tracing in terms of 4×4 matrices in ray-centered coordinates

$$\frac{d\mathbf{\Pi}}{dT} = \mathbf{S}\mathbf{\Pi}, \tag{8}$$

with the initial condition

$$\mathbf{\Pi}^0 = \begin{pmatrix} \mathbf{I} & \mathbf{0} \\ \mathbf{0} & \mathbf{I} \end{pmatrix}. \tag{9}$$

Here, $\mathbf{\Pi}$ is the ray propagator matrix with submatrices of size 2×2,

$$\mathbf{\Pi} = \begin{pmatrix} \mathbf{Q}_1 & \mathbf{Q}_2 \\ \mathbf{P}_1 & \mathbf{P}_2 \end{pmatrix}. \tag{10}$$

As is well known, the first and second set of paraxial matrices, $(\mathbf{Q}_1, \mathbf{P}_1)$ and $(\mathbf{Q}_2, \mathbf{P}_2)$, can be interpreted as plane-wave (or telescopic) and point-source components of the propagator matrix $\mathbf{\Pi}$ (see, for example, Červený, 2001). Because image rays correspond to an initial plane wave, the relevant set of paraxial matrices is $(\mathbf{Q}_1, \mathbf{P}_1)$. Matrix $\mathbf{S}$ in equation 8 has the definition

$$\mathbf{S} = \begin{pmatrix} \mathbf{0} & v^2\mathbf{I} \\ -v^{-1}\mathbf{V} & \mathbf{0} \end{pmatrix}, \quad \text{where } \mathbf{V} = \left(\frac{\partial^2 v}{\partial q_I \partial q_J} \right). \tag{11}$$

Relating time- and depth-domain velocity functions

To simplify the notation, we shall consider in the following three velocity functions, all of them denoted by the letter v, and distinguished solely by their arguments: $v(\mathbf{x})$, $v(\boldsymbol{\gamma})$, and $v(\mathbf{q})$. More specifically, $v(\mathbf{x})$ and $v(\boldsymbol{\gamma})$ will designate the depth-domain velocity in global Cartesian coordinates and ray coordinates, respectively. In a standard forward ray-tracing application, that is, when image rays are computed from a known velocity field $v(\mathbf{x})$, the velocity $v(\boldsymbol{\gamma})$ can be obtained for each ray (for which the first two components, $\overline{\boldsymbol{\gamma}} = (\gamma_1, \gamma_2)^T$ are fixed) simply by assigning the value $v(\mathbf{x})$ at each position $\mathbf{x}$ on the ray to the corresponding coordinate vector $\boldsymbol{\gamma}$. Finally, for any selected point on the ray, $v(\mathbf{q})$ defines the velocity in the local Cartesian coordinate system.

As shown in Appendix C, the ray-domain velocity $v(\boldsymbol{\gamma})$ will be given by

$$v(\boldsymbol{\gamma}) = v^M_{\text{dix}}(\boldsymbol{\gamma}) F(\boldsymbol{\gamma}), \tag{12}$$

where F, referred to as the velocity spreading factor, is given by

$$F(\boldsymbol{\gamma}) = \frac{\overline{\mathbf{u}}^T \mathbf{Q}_2^{-1} \mathbf{Q}_1 \overline{\mathbf{u}}}{\{\overline{\mathbf{u}}^T \mathbf{Q}_2^{-1} \mathbf{Q}_2^{-T} \overline{\mathbf{u}}\}^{1/2}}. \tag{13}$$

In the 2D situation, the factor F reduces to the simple formula

$$F(\boldsymbol{\gamma}) = Q_1, \tag{14}$$

where Q_1 is the scalar that corresponds in 2D propagation to the 2×2 transformation matrix $\mathbf{Q}_1$, which refers to the 3D situation. Equation 14 is equal to the one given in Cameron et al. (2006, 2007).

We note that although v^M_{dix} is directly available as input, the factor F depends on quantities belonging to dynamic ray tracing along the image ray. This means our image-ray construction must contemplate a simultaneous solution of the kinematic and dynamic ray-tracing systems.

Derivatives of velocity functions

We now address the problem of determining the velocity derivatives $\partial v/\partial \mathbf{x}$ and $\partial^2 v/\partial \overline{\mathbf{q}}^2$ that are needed in the kinematic and dynamic ray-tracing systems formulated above. These will be given in terms of the ray-domain velocity derivatives, $\partial v/\partial \boldsymbol{\gamma}$ and $\partial^2 v/\partial \overline{\boldsymbol{\gamma}}^2$, respectively. The latter derivatives are related closely to the corresponding derivatives of our input time-migration interval velocity field v^M_{dix}.

For first-order derivatives, a simple application of the chain rule of advanced calculus yields

$$\frac{\partial v}{\partial \gamma_i} = \frac{\partial x_k}{\partial \gamma_i} \frac{\partial v}{\partial x_k} \tag{15}$$

and introduces the matrix

$$\hat{\mathbf{Q}}_1^{(x)} = \left(\frac{\partial x_i}{\partial \gamma_j} \right) \tag{16}$$

of the transformation between ray coordinates $(\boldsymbol{\gamma}_j)$ and global Cartesian coordinates (x_i). Furthermore, one can relate matrix $\hat{\mathbf{Q}}_1^{(x)}$ to its counterpart, $\hat{\mathbf{Q}}_1^{(q)} = (\partial q_i/\partial \gamma_j)$, in local Cartesian coordinates by the transformation

$$\hat{\mathbf{Q}}_1^{(x)} = \hat{\mathbf{H}} \hat{\mathbf{Q}}_1^{(q)}, \quad \text{where } \hat{\mathbf{Q}}_1^{(q)} = \begin{pmatrix} & & 0 \\ & \mathbf{Q}_1 & 0 \\ 0 & 0 & v \end{pmatrix}. \tag{17}$$

We recall that $\hat{\mathbf{H}}$ is the 3×3 matrix given by equation 5, and $\mathbf{Q}_1$ is the 2×2 upper left submatrix of the 4×4 ray-centered propagator matrix $\mathbf{\Pi}$ of equation 10. Under the assumption that the inverse matrix, $(\hat{\mathbf{Q}}_1^{(x)})^{-1} = (\partial \gamma_i/\partial x_j)$ exists (or, equivalently, that $\det \hat{\mathbf{Q}}^{(x)} \neq 0$), equation 15 can be recast as

$$\frac{\partial v}{\partial \mathbf{x}} = (\hat{\mathbf{Q}}_1^{(x)})^{-T} \frac{\partial v}{\partial \boldsymbol{\gamma}}. \tag{18}$$

The existence of the inverse matrix $(\hat{\mathbf{Q}}_1^{(x)})^{-1}$ for all considered values of the ray-coordinate vector $\boldsymbol{\gamma}$ ensures a one-to-one correspondence between ray coordinates and depth-domain coordinates, $\mathbf{x} = \mathbf{x}(\boldsymbol{\gamma})$ and $\boldsymbol{\gamma} = \boldsymbol{\gamma}(\mathbf{x})$. Thus, in this particular situation, each point in the depth domain is connected to the measurement surface by at most one image ray only, and the image-ray field does not contain caustic points. We remark in passing that the condition $\det \hat{\mathbf{Q}}_1^{(x)} \neq 0$ has to be fulfilled in any implementation of the image-ray construction considered here. To obtain the relationship between the second derivatives of velocity in ray coordinates and local Cartesian coordinates, the chain rule needs to be applied twice.

As shown in Appendix D, we have

$$\frac{\partial^2 v}{\partial q_N \partial q_M} = \frac{\partial \gamma_I}{\partial q_N}\frac{\partial \gamma_J}{\partial q_M}\left(\frac{\partial^2 v}{\partial \gamma_I \partial \gamma_J} - \frac{\partial^2 q_K}{\partial \gamma_I \partial \gamma_J}\frac{\partial v}{\partial q_K}\right) + M_{NM}\frac{\partial v}{\partial T}, \quad (19)$$

where $M_{NM} = \partial^2 T/\partial q_N \partial q_M$. At this point, it is essential to emphasize that conventional dynamic ray tracing for a single ray does not allow computation of derivatives of q_K of orders two and higher. Hence, we can conclude that if the procedure is to be based on computations along a single ray only, we have to assume that such derivatives have negligible values. Given that this assumption is satisfied, equation 19 can be approximated by the simpler matrix expression,

$$\frac{\partial^2 v}{\partial \bar{\mathbf{q}}^2} = \mathbf{Q}_1^{-T}\frac{\partial^2 v}{\partial \bar{\boldsymbol{\gamma}}^2}\mathbf{Q}_1^{-1} + \mathbf{M}_1\frac{\partial v}{\partial T}, \quad (20)$$

where $\mathbf{M}_1 = \partial^2 T/\partial \bar{\mathbf{q}}^2 = \mathbf{P}_1\mathbf{Q}_1^{-1}$. Equations 18 and 19 (or equation 20) provide the link between the first and second derivatives of velocity with respect to ray coordinates and the corresponding velocity derivatives with respect to global Cartesian coordinates and ray-centered coordinates, respectively. As seen in the next section, this link will be crucial for the image-ray tracing and velocity-estimation algorithm that is proposed here.

Numerical integration along the image ray

Collecting results, the complete set of ordinary differential equations integrated to obtain the image ray is specified by equation 4, 6, and 8. As input to the evaluation of the right-hand side of the differential equations, we have the independent variable along the ray, T, and the set of dependent variables, $\mathbf{x}$, $\mathbf{p}$, $\mathbf{e}_1$, and $\mathbf{\Pi}$. We also need as input the horizontal coordinates of the starting point of the image ray, x_I^{M0}; the unit vector corresponding to the migration azimuth, $\bar{\mathbf{u}}$; and the time-migration interval velocity field, $v_{\text{dix}}^M(\boldsymbol{\gamma})$. An important part of the procedure is on-the-fly transformation of function values, first derivatives, and second derivatives belonging to the time-migration interval velocity field, $v_{\text{dix}}^M(\boldsymbol{\gamma})$, to corresponding quantities in the ray-domain velocity field, $v(\boldsymbol{\gamma})$. For a better appreciation of the numerical integration scheme that is central to our time-to-depth conversion algorithm, we have specified in Table 2 the sequence of computational operations involved in evaluating the differential equations. It has been assumed that derivatives along a ray of ray-centered coordinates, q_K, of higher order than one in the ray parameters, γ_I, can be neglected.

For the isotropic conditions under consideration, the ray-domain velocity can be obtained, besides from equation 12, as the inverse length of the slowness vector, $v = \|\mathbf{p}\|^{-1}$. This provides a possibility of checking the numerical accuracy during integration of the differential equations. For details concerning computation of velocity derivatives along the image ray, see Appendix E.

Table 2. Proposed sequence of computational steps involved in evaluating the right-hand side of the system of ray differential equations.

Step number	Description	Equation number
1	Form the vector $\boldsymbol{\gamma} = (\gamma_1, \gamma_2, T)^T$, where $\gamma_1 = x_1^{M0}$ and $\gamma_2 = x_2^{M0}$ are fixed for all computations along the ray.	
2	Evaluate the time-migration interval velocity, v_{dix}^M, and its derivatives, $\partial v_{\text{dix}}^M/\partial \gamma_I$ and $\partial^2 v_{\text{dix}}^M/\partial \gamma_I \partial \gamma_J$.	
3	Calculate the factors A, B, and F: $A = \bar{\mathbf{u}}^T\mathbf{Q}_2^{-1}\mathbf{Q}_1\bar{\mathbf{u}}$, $B = \bar{\mathbf{u}}^T\mathbf{Q}_2^{-1}\mathbf{Q}_2^{-T}\bar{\mathbf{u}}$, and $F = A/B^{1/2}$.	E-4, E-5
4	Establish the depth-domain velocity, $v = v_{\text{dix}}^M F$.	12
5	Evaluate the differential equations $d\mathbf{x}/dT = v^2\mathbf{p}$, $d\mathbf{Q}_I/dT = v^2\mathbf{P}_I$.	4, 8, 10, 11
6	Find the two remaining basis vectors of the local Cartesian coordinate system, using $\mathbf{e}_3 = \mathbf{p}/\|\mathbf{p}\|$ and $\mathbf{e}_2 = \mathbf{e}_3 \times \mathbf{e}_1$. This yields the transformation matrix $\hat{\mathbf{H}} = (\mathbf{e}_1\ \mathbf{e}_2\ \mathbf{e}_3)$.	7, 5
7	Use the transformation $\hat{\mathbf{Q}}^{(x)} = \hat{\mathbf{H}}\hat{\mathbf{Q}}^{(q)}$.	3, 17
8	Find derivatives of the factors A, B, and F, using the equations $\partial A/\partial T = -v^2\bar{\mathbf{u}}^T\mathbf{Q}_2^{-1}\mathbf{Q}_2^{-T}\bar{\mathbf{u}} = -v^2 B$, $\partial B/\partial T = -2v^2\bar{\mathbf{u}}^T\mathbf{Q}_2^{-1}\mathbf{P}_2\mathbf{Q}_2^{-1}\mathbf{Q}_2^{-T}\bar{\mathbf{u}}$, and $\partial F/\partial T = (\partial A/\partial T)B^{1/2} - (\partial B/\partial T)(A/2)B^{-3/2}$.	E-6, E-6, E-5
9	Apply approximations for derivatives of factor F along the ray, which yields $\partial v/\partial \gamma_I = \partial v_{\text{dix}}^M/\partial \gamma_I F$ and $\partial v/\partial T = \partial v_{\text{dix}}^M/\partial T\, F + v_{\text{dix}}^M \partial F/\partial T$.	E-3
10	Obtain the velocity gradient in depth-domain Cartesian coordinates by $\partial v/\partial \mathbf{x} = (\hat{\mathbf{Q}}^{(x)})^{-T}\partial v/\partial \boldsymbol{\gamma}$.	18
11	Evaluate the differential equations for the vectors $\mathbf{p}$ and $\mathbf{e}_1$, $d\mathbf{p}/dT = -v^{-1}\partial v/\partial \mathbf{x}$, $d\mathbf{e}_1/dT = -v^2(\mathbf{e}_1 \cdot d\mathbf{p}/dT)\mathbf{p}$.	4, 6
12	Find the approximate second derivatives $\partial^2 v/\partial \gamma_I \partial \gamma_J = (\partial^2 v_{\text{dix}}^M/\partial \gamma_I \partial \gamma_J)F$ and apply the transformation $\partial^2 v/\partial \bar{\mathbf{q}}^2 = \mathbf{Q}_1^{-T}(\partial^2 v/\partial \bar{\boldsymbol{\gamma}}^2)\mathbf{Q}_1^{-1} + \mathbf{M}_1(\partial v/dT)$, with $\mathbf{M}_1 = \mathbf{P}_1\mathbf{Q}_1^{-1}$.	E-3, D-10
13	As a final step, evaluate the differential equations for matrices $\mathbf{P}_I$ by $d\mathbf{P}_I/dT = -v^{-1}\mathbf{V}\mathbf{Q}_I$.	8, 10, 11

Initial conditions for tracing the image ray

To solve the kinematic and dynamic ray-tracing systems, initial conditions have to be provided. These consist of initial values, $\mathbf{x}^0$, $\mathbf{p}^0$, $\mathbf{e}_1^0$, and $\mathbf{\Pi}^0$, given for the initial ray coordinate vector $\boldsymbol{\gamma}^0 = (\gamma_1^0, \gamma_2^0, \gamma_3^0)^T$. Assuming for simplicity a planar horizontal datum surface, $x_3 = 0$, for the time-migrated data, we set $\gamma_1^0 = x_1^{M0}$, $\gamma_1^0 = x_2^{M0}$ as the horizontal coordinates of the starting point of the image ray. The given pair (x_1^{M0}, x_2^{M0}) also specifies the trace location in the time-migrated data set that corresponds to the image ray to be constructed. The initial traveltime of the image ray is $\gamma_3^0 = T^0 = 0$.

Because the initial slowness vector of an image ray $\mathbf{p}^0$ is always perpendicular to the measurement surface, the two horizontal slowness vector components will both be zero, that is, $p_1^0 = p_2^0 = 0$. The vertical slowness vector component is given by the inverse ray-domain velocity, $p_3^0 = 1/v_0$, at the trace location (x_1^{M0}, x_2^{M0}) and zero migration time, $t^{M0} = 2T^0 = 0$. Furthermore, one can show (Appendix E) that the factor F in equation 13 has the limit one when the migration time approaches zero. Hence, equation 12 yields the initial ray-domain velocity as

$$v^0 = v_{\mathrm{dix}}^M(\boldsymbol{\gamma}^0). \tag{21}$$

Given the above specifications, the kinematic initial conditions for the image ray read

$$\mathbf{x}^0 = (x_1^{M0}, x_2^{M0}, 0)^T \text{ and } \mathbf{p}^0 = \left(0, 0, \frac{1}{v^0}\right)^T. \tag{22}$$

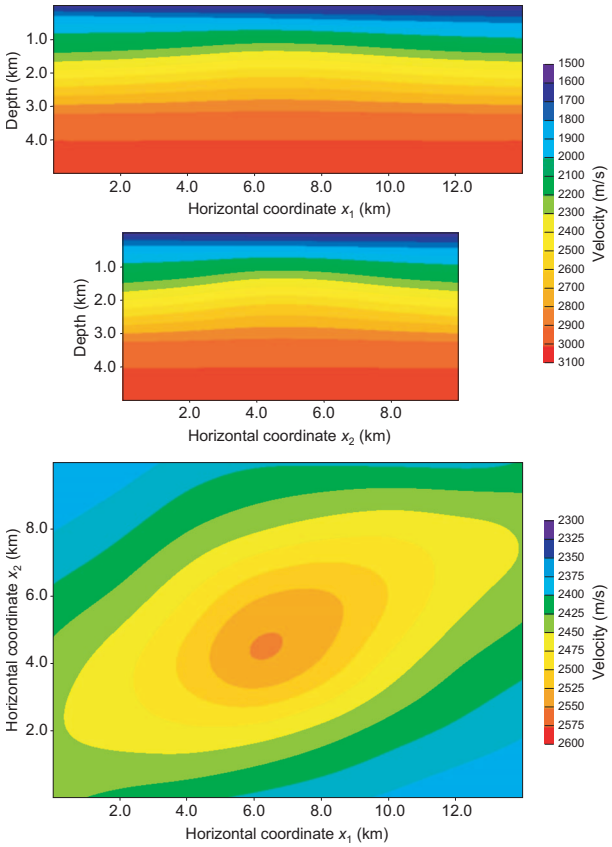

Figure 2. Depth-domain velocity used for generating input data for the tests. Top: section $x_2 = 5$ km. Middle: section $x_1 = 7$ km. Bottom: depth slice $x_3 = 2$ km.

The initial unit vector $\mathbf{e}_1^0$ of the ray-centered coordinate system can be chosen quite freely within the horizontal plane. One option is to align it with the migration azimuth direction, in other words, to specify $\mathbf{e}_1^0 = (\cos\theta, \sin\theta, 0)^T$. The initial ray-propagator matrix, $\mathbf{\Pi}^0$, is the 4×4 identity matrix given by equation 9.

NUMERICAL EXAMPLES

In this section, we consider, as a first illustration of the method, examples based on a 3D model of the subsurface. Three cross sections through the P-wave velocity field of this model are shown in Figure 2. The velocity field contains mild lateral variations and is smooth throughout; that is, it has no interfaces, discontinuities, or areas without data.

To obtain input data for the numerical tests, image rays were traced a one-way time $T = 2$ s downward from a planar measurement surface, located at depth $x_3 = 0$ km. Figure 3 shows image rays projected into the three global Cartesian coordinate directions. One can observe deviations of rays from the vertical. Nevertheless, the velocity variations responsible for these deviations do not introduce triplications and caustics in the image-ray field. To facilitate display and comparisons of velocities, positions, and their errors, we show in the following all results as functions of the coordinates of the time-migration domain. As an introduction to this type of display, consider Figure 4, which shows the "true" depth-domain velocity posted along the generated image rays.

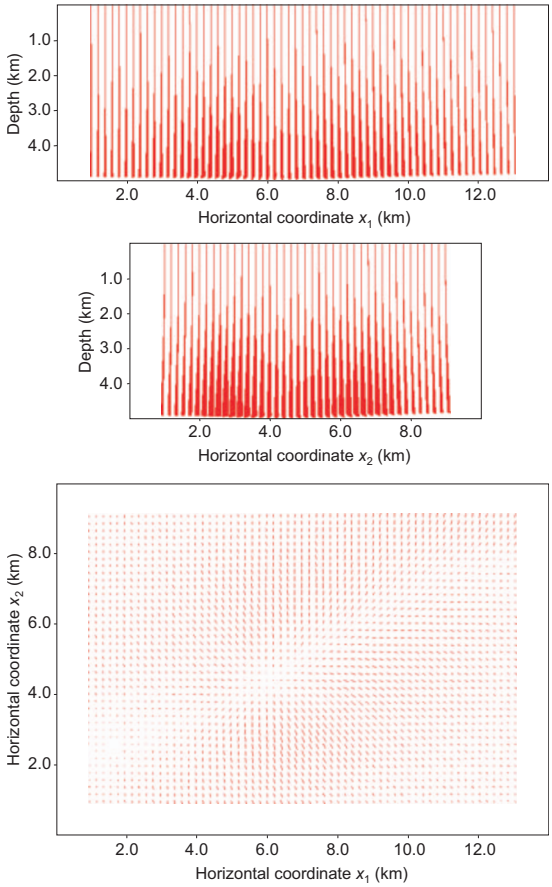

Figure 3. Projections of image rays in (top) x_2 direction, (middle) x_1 direction, and (bottom) x_3 direction.

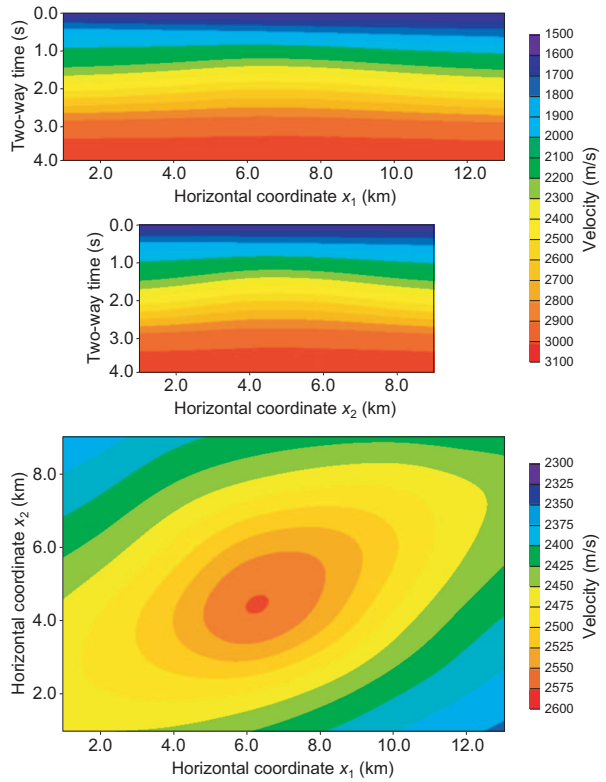

Figure 4. Depth-domain velocity as a function of time-domain coordinates. Top: section $x_2 = 5$ km. Middle: section $x_1 = 7$ km. Bottom: time slice $t^M = 2$ s.

By calculating the ray-propagator matrix along the rays, we obtained as a by-product the matrix of second derivatives of the one-way diffraction time, which contains information about migration velocity for any azimuth θ. Thereafter, we specifically selected the migration velocity field corresponding to the azimuth $\theta = 0°$ (Figure 5) and converted it to a time-migration interval velocity field (Figure 6), using Dix's method (see equation 3). The reason for calculating the input data in this way was to attain control of errors resulting from the image-ray transformation alone. We remark in passing that an equivalent approach to obtaining time-migration interval velocities is to use equation C-11.

The experiments were conducted with two transformations relating the time and depth domains. One approach was established by neglecting all lateral variations of the time-migration interval velocity. Because this action results in vertical image rays, we refer to it as vertical-ray transformation. The other approach is based on the methodology for the image-ray transformation presented in this paper but with the underlying assumption that the derivatives of ray-centered coordinates along a ray, q_K, of higher order than one in the ray parameters, γ_I, can be neglected.

Considering first the vertical-ray transformation, Figure 7 shows errors in the estimation of the position (x_i) for a selected time slice, $t^M = 2$ s. The corresponding errors resulting from the image-ray transformation are shown in Figure 8. The latter displays can be

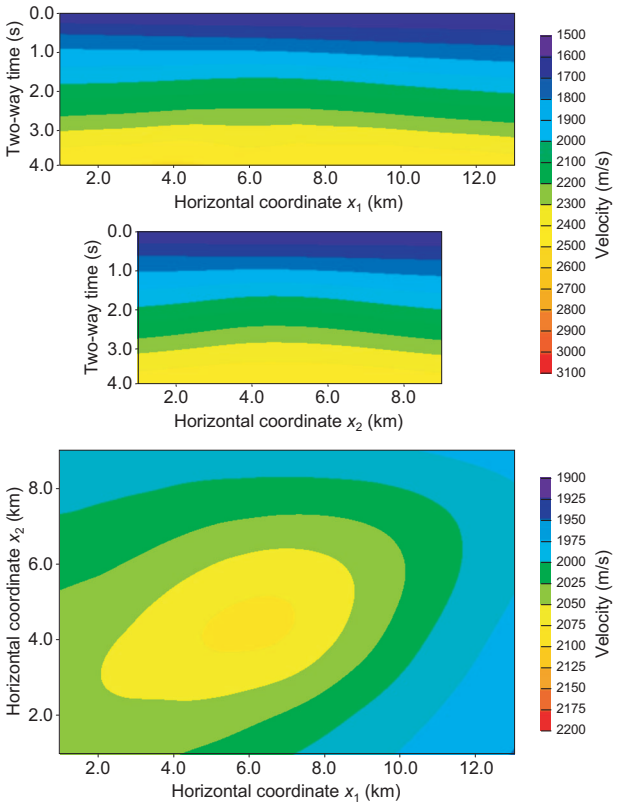

Figure 5. Time-migration velocity as a function of time-domain coordinates. Top: section $x_2^M = 5$ km. Middle: section $x_1^M = 7$ km. Bottom: time slice $t^M = 2$ s.

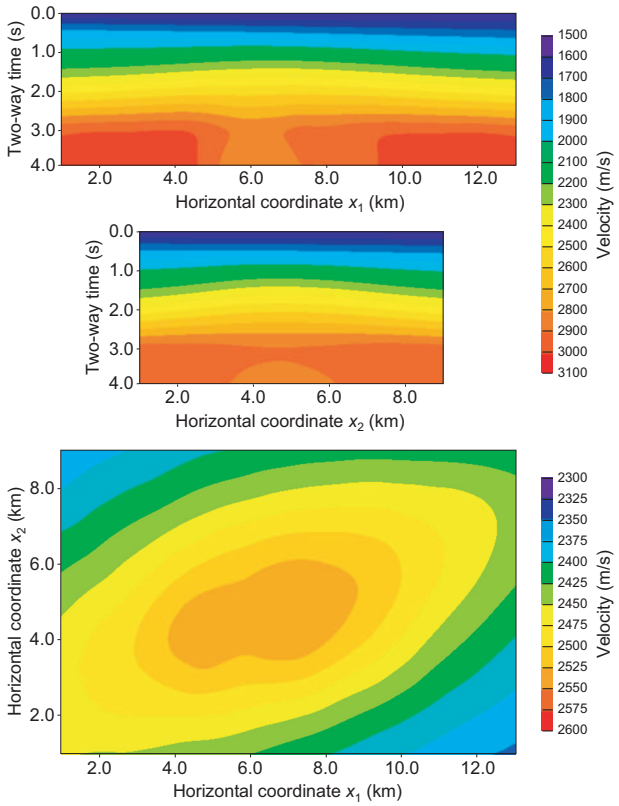

Figure 6. Time-migration interval velocity as a function of time-domain coordinates. Top: section $x_2^M = 5$ km. Middle: section $x_1^M = 7$ km. Bottom: time slice $t^M = 2$ s.

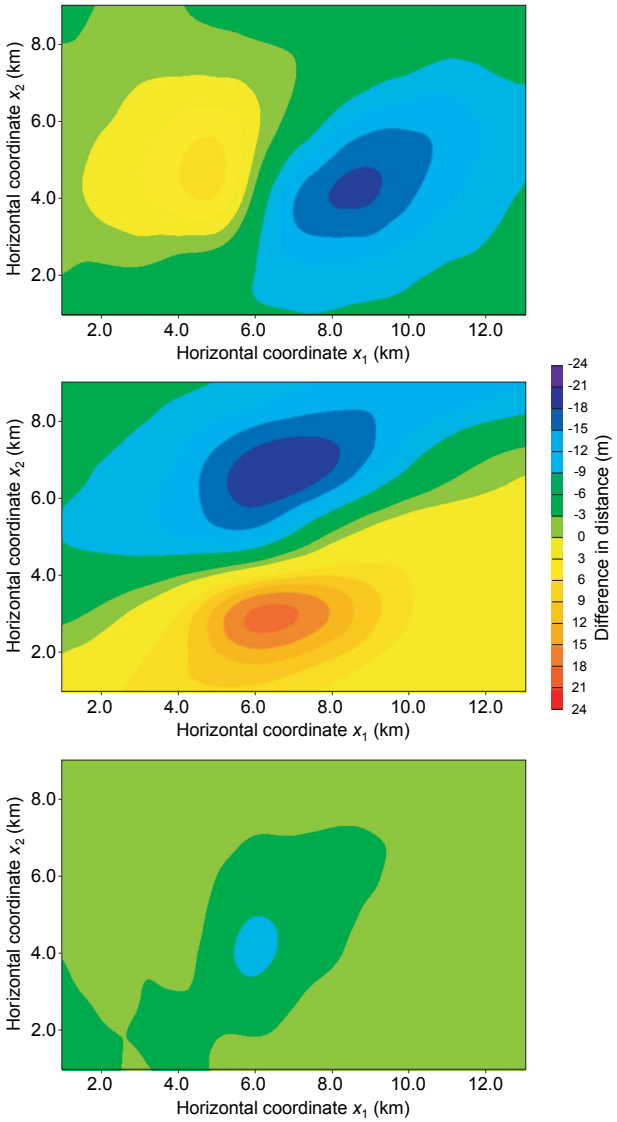

Figure 7. Vertical-ray transformation approach. Depth-domain position errors for time slice $t^M = 2$ s. Coordinates (top) x_1, (middle) x_2, and (bottom) x_3.

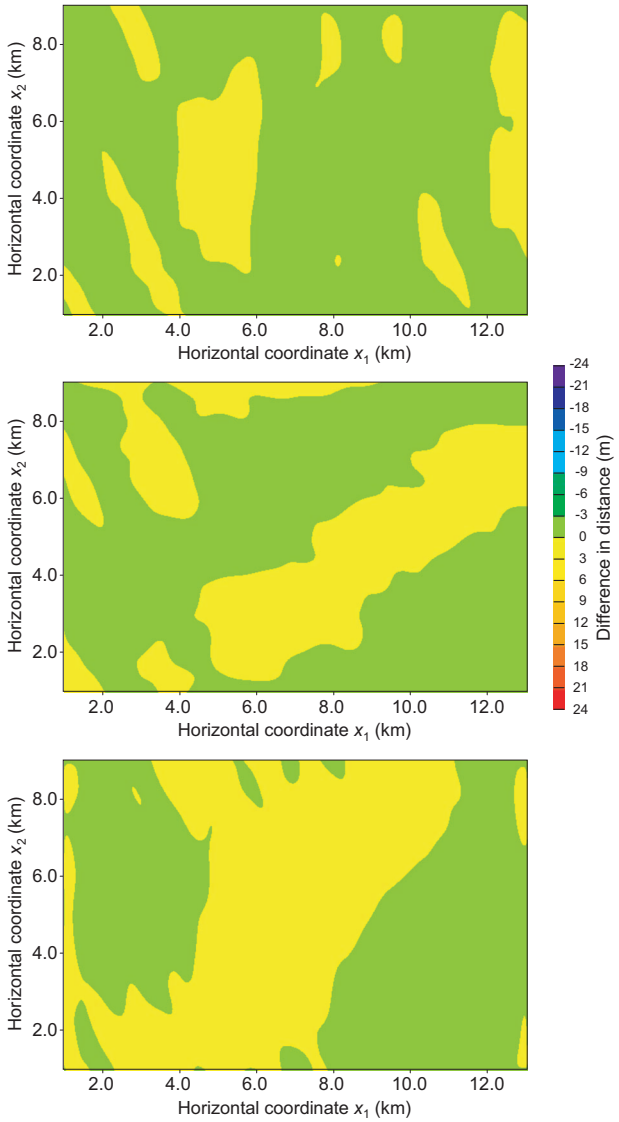

Figure 8. Image-ray transformation approach. Depth-domain position errors for time slice $t^M = 2$ s. Errors of coordinates (top) x_1, (middle) x_2, and (bottom) x_3.

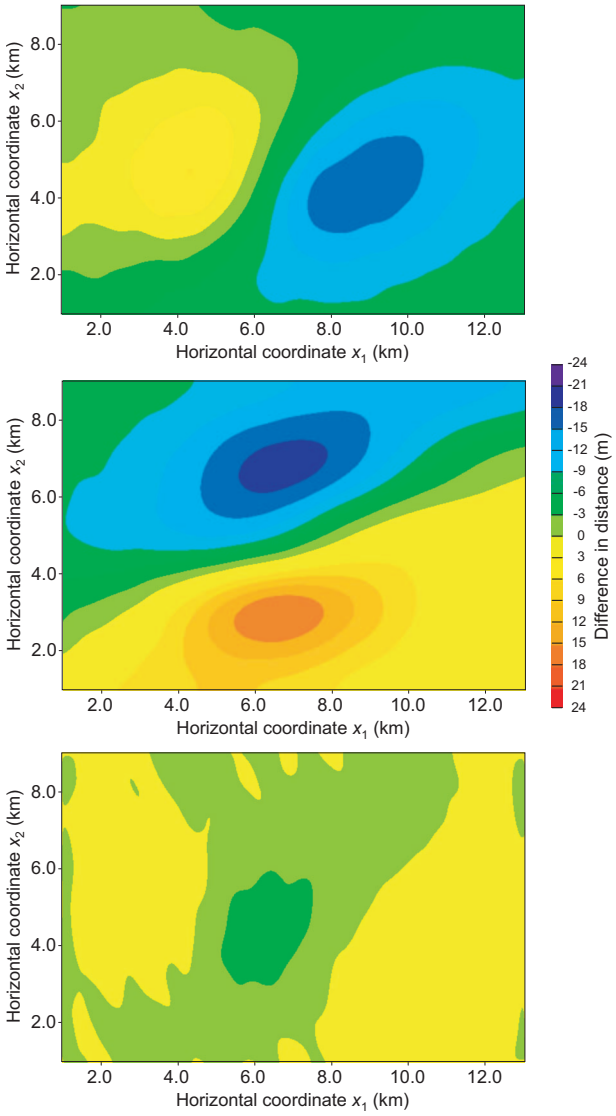

Figure 9. Vertical-ray versus image-ray transformation approaches. Depth-domain position differences for time slice $t^M = 2$ s. Differences in coordinates (top) x_1, (middle) x_2, and (bottom) x_3.

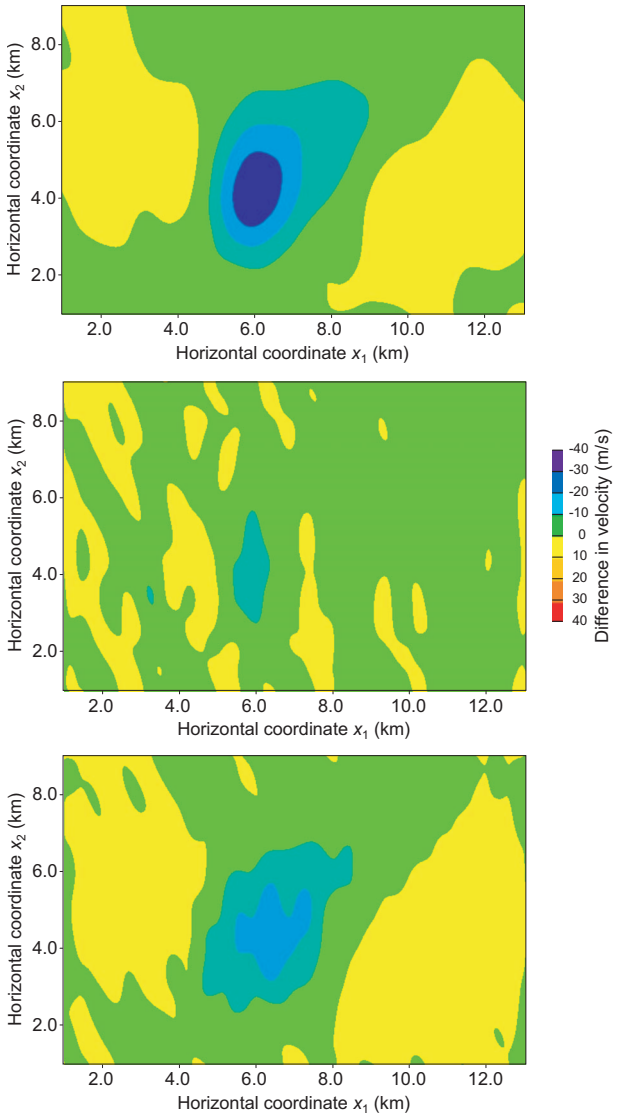

Figure 10. Comparisons of depth-domain velocities for time slice $t^M = 2$ s. Error using (top) vertical-ray and (middle) image-ray transformation. Bottom: difference between vertical-ray and image-ray transformations. Velocity differences in the top, middle, and bottom subfigures correspond, respectively, to the position differences in Figures 7–9.

interpreted as estimated time-to-depth conversion errors for a virtual flat horizon in the time-migration domain. A possibility of direct comparison between the vertical-ray and image-ray transformations is provided in Figure 9. It can be concluded that errors arising from the applied image-ray transformation are smaller than those of the vertical-ray transformation, particularly with regard to the error in lateral positioning. In Figure 10, one can compare the accuracy of the depth-domain velocities obtained by the two approaches. Again, the image-ray transformation generally yields smaller errors. We remark, however, that this approach is quite sensitive to the smoothness of the first- and second-order derivatives of the time-migration interval velocity field.

CONCLUSIONS

Starting from a given 3D time-migration velocity field, available for a single migration azimuth, we have presented an efficient scheme to trace image rays and simultaneously to estimate the velocity along them. The obtained velocities can provide, after regularization, a depth-domain velocity field that can be useful for many seismic applications. These include, for example, the use of the estimated velocity field as a macrovelocity model for depth migration or as an initial model for tomographic inversion. The proposed scheme also provides the basis for time-to-depth conversion without the need for a priori information of the depth-domain velocity model.

We have benefited greatly from recent investigations that establish the link between the time-migration interval velocity and the corresponding velocity along the image ray. The resulting algorithm for 3D image-ray tracing into depth uses a time-migration velocity field known in three azimuths. In this paper, besides reviewing the literature, we have introduced an alternative algorithm, which requires knowledge of the time-migration velocity field in only a single azimuth. As a consequence, we foresee that our approach will be easier to use in practice. The new algorithm has been applied and discussed on a 3D synthetic example. An overall impression from this first test is that errors generated by the developed image-ray transformation are smaller than those of the classic vertical-ray transformation, particularly concerning lateral positioning.

The present scheme is bound to yield best results whenever time migration provides sufficient focusing and a reliable time-migration velocity field. As its main advantage, it delivers a direct estimation of the depth-domain velocity with a minimum of user interaction/intervention. The method is very efficient as compared, for example, with full prestack depth migration and associated estimation of depth-domain velocity parameters. The constraints or limitations of the proposed procedure are those basically inherited by the use of time migration, the ray method, and Dix's type velocity inversions. For adequate ray-tracing implementation, the time-migration interval velocity function and its first-and second-order derivatives all need to be "sufficiently smooth." Moreover, the resolution in the velocity estimation is expected to be poor for deep and/or thin "layers." As an additional condition for effective implementation, care should be taken so that the image-ray field has no triplications and caustics.

ACKNOWLEDGMENTS

We thank F. Adler, S. Fomel, I. Pšenčík, J. A. Sethian, and one anonymous reviewer for constructive criticism and helpful suggestions. E. Iversen acknowledges support from the Research Council of Norway (project 174549/S30), StatoilHydro, and NORSAR. In particular, he is grateful to his colleagues K. Åstebøl and H. Gjøystdal for a fruitful collaboration on the topic of time-to-depth conversion along image rays in the late 1980s. The work performed at that time was not published as a regular paper, but essential results were presented at an EAEG meeting and in a NORSAR report (these are cited in the reference list of this paper as Iversen et al., 1987, and Iversen et al., 1988, respectively). M. Tygel acknowledges support from the National Council of Scientific and Technological Development (CNPq), Brazil, and the Research Foundation of the State of São Paulo (FAPESP), Brazil. This work also has been supported by the sponsors of the Wave Inversion Technology (WIT) Consortium, Karlsruhe, Germany.

APPENDIX A

3D KIRCHHOFF PRESTACK TIME MIGRATION

As explained in the introduction, Kirchhoff time migration and time-migration velocity analysis are realized in the same way as a CMP stacking and velocity analysis, under the use of an appropriate traveltime operator. This operator is the hyperbolic diffraction traveltime defined below. For more information on the conceptual and practical aspects of time migration, we refer to Hubral and Krey (1980), Yilmaz (2001), and Robein (2003).

HYPERBOLIC DIFFRACTION TIME APPROXIMATION

Let $\mathbf{s}$ and $\mathbf{r}$ denote the three-component position vectors for the source and receiver, respectively. In addition, define $\bar{\mathbf{s}} = (s_1, s_2)^T$ and $\bar{\mathbf{r}} = (r_1, r_2)^T$, and assume $s_3 = r_3 = 0$. We also introduce the midpoint vector, $\bar{\mathbf{x}} = (x_1, x_2)^T$, and the half-offset vector, $\bar{\mathbf{y}} = (y_1, y_2)^T$. Observe that for the cause of clarity, we do not distinguish the notation of midpoint vector components and global Cartesian coordinates. The vectors $\bar{\mathbf{s}}$ and $\bar{\mathbf{r}}$ are expressed in terms of the vectors $\bar{\mathbf{x}}$ and $\bar{\mathbf{y}}$ by

$$\bar{\mathbf{s}} = \bar{\mathbf{x}} + \bar{\mathbf{y}}, \quad \bar{\mathbf{r}} = \bar{\mathbf{x}} - \bar{\mathbf{y}}. \tag{A-1}$$

Let vector $\bar{\mathbf{x}}^M$ define a location onto which contributions from trace $(\bar{\mathbf{s}}, \bar{\mathbf{r}})$ will be migrated. Introducing the migration aperture vector $\bar{\mathbf{a}}$ as

$$\bar{\mathbf{a}} = \bar{\mathbf{x}} - \bar{\mathbf{x}}^M, \tag{A-2}$$

we can write

$$\bar{\mathbf{s}} - \bar{\mathbf{x}}^M = \bar{\mathbf{a}} + \bar{\mathbf{y}}, \quad \bar{\mathbf{r}} - \bar{\mathbf{x}}^M = \bar{\mathbf{a}} - \bar{\mathbf{y}}. \tag{A-3}$$

One-way times from a diffraction point $\mathbf{x}^D$ in the subsurface to the source and receiver points $\mathbf{s}$ and $\mathbf{r}$ now can be expressed by the second-order approximations

$$t^s(\bar{\mathbf{s}}, \mathbf{x}^D) = t^s(\bar{\mathbf{x}}^M, \mathbf{x}^D) + (\bar{\mathbf{p}}^{s(x)})^T(\bar{\mathbf{s}} - \bar{\mathbf{x}}^M) + \frac{1}{2}(\bar{\mathbf{s}} - \bar{\mathbf{x}}^M)^T \mathbf{M}^{s(x)}(\bar{\mathbf{s}} - \bar{\mathbf{x}}^M), \tag{A-4}$$

$$t^r(\bar{\mathbf{r}}, \mathbf{x}^D) = t^r(\bar{\mathbf{x}}^M, \mathbf{x}^D) + (\bar{\mathbf{p}}^{r(x)})^T(\bar{\mathbf{r}} - \bar{\mathbf{x}}^M) + \frac{1}{2}(\bar{\mathbf{r}} - \bar{\mathbf{x}}^M)^T \mathbf{M}^{r(x)}(\bar{\mathbf{r}} - \bar{\mathbf{x}}^M). \tag{A-5}$$

The vectors $\bar{\mathbf{p}}^{s(x)}$ and $\bar{\mathbf{p}}^{r(x)}$ have components

$$p_I^{s(x)} = \frac{\partial t^s}{\partial s_I}, \quad p_I^{r(x)} = \frac{\partial t^r}{\partial r_I}, \tag{A-6}$$

evaluated at $\bar{\mathbf{s}} = \bar{\mathbf{x}}^M$ and $\bar{\mathbf{r}} = \bar{\mathbf{x}}^M$, respectively. The 2×2 matrices $\mathbf{M}^{s(x)}$ and $\mathbf{M}^{r(x)}$ have elements

$$[\mathbf{M}^{s(x)}]_{IJ} = \frac{\partial^2 t^s}{\partial s_I \partial s_J}, \quad [\mathbf{M}^{r(x)}]_{IJ} = \frac{\partial^2 t^r}{\partial r_I \partial r_J}, \tag{A-7}$$

also evaluated for $\bar{\mathbf{s}} = \bar{\mathbf{x}}^M$ and $\bar{\mathbf{r}} = \bar{\mathbf{x}}^M$, respectively.

A second-order approximation to the diffraction time now can be formed as

$$t^D(\bar{\mathbf{s}}, \bar{\mathbf{r}}, \mathbf{x}^D) = t^s(\bar{\mathbf{s}}, \mathbf{x}^D) + t^r(\bar{\mathbf{r}}, \mathbf{x}^D). \tag{A-8}$$

We assume that traveltimes t^s and t^r correspond to the same elementary wave mode, for example, a direct P-wave. This means that $t^s(\bar{\mathbf{x}}^M, \mathbf{x}^D) = t^r(\bar{\mathbf{x}}^M, \mathbf{x}^D)$, $\bar{\mathbf{p}}^{s(x)} = \bar{\mathbf{p}}^{r(x)}$, and $\mathbf{M}^{s(x)} = \mathbf{M}^{r(x)}$. For convenience, the latter quantities thus are written in the following without superscripts s and r. Assume in addition that $\mathbf{x}^M$ is a stationary point for the diffraction time. This has the consequence

$$\bar{\mathbf{p}}^{s(x)} + \bar{\mathbf{p}}^{r(x)} = 2\bar{\mathbf{p}}^{(x)} = 0. \tag{A-9}$$

By squaring equation A-8, neglecting terms of order three and higher, and applying the transformations in equation A-3, we obtain the following hyperbolic approximation to the diffraction time:

$$t^D(\bar{\mathbf{x}}^M,t^M,\bar{\mathbf{a}},\bar{\mathbf{y}})^2 = t^{M^2} + 2t^M[\bar{\mathbf{a}}^T\mathbf{M}^{(x)}(\bar{\mathbf{x}}^M,t^M)\bar{\mathbf{a}} + \bar{\mathbf{y}}^T\mathbf{M}^{(x)}(\bar{\mathbf{x}}^M,t^M)\bar{\mathbf{y}}]. \quad \text{(A-10)}$$

Here, t^M is the two-way time between the points $\mathbf{x}^D$ and $\mathbf{x}^M$, i.e.,

$$t^M = 2t(\bar{\mathbf{x}}^M,\mathbf{x}^D). \quad \text{(A-11)}$$

Equation A-10 is equivalent to equation 11.4 in Hubral and Krey (1980), the only difference being that the half-offset vector is defined with opposite sign.

Introducing the notation $\bar{\mathbf{u}}(\theta) = (\cos\theta,\sin\theta)^T$, let us now write

$$\bar{\mathbf{a}} = a\bar{\mathbf{u}}(\theta_a), \quad \bar{\mathbf{y}} = y\bar{\mathbf{u}}(\theta_y), \quad \text{(A-12)}$$

with $a = \|\bar{\mathbf{a}}\|$ and $y = \|\bar{\mathbf{y}}\|$ and define the direction-dependent migration velocity by the equation

$$[v^M(\bar{\mathbf{x}}^M,t^M,\theta)]^2 = \frac{2}{t^M\bar{\mathbf{u}}(\theta)^T\mathbf{M}^{(x)}(\bar{\mathbf{x}}^M,t^M)\bar{\mathbf{u}}(\theta)}, \quad \text{(A-13)}$$

in accordance with equation 11.3 of Hubral and Krey (1980). This yields

$$t^D(\bar{\mathbf{x}}^M,t^M,a,y,\theta_a,\theta_y)^2 = t^{M^2} + \frac{4a^2}{[v^M(\bar{\mathbf{x}}^M,t^M,\theta_a)]^2} + \frac{4y^2}{[v^M(\bar{\mathbf{x}}^M,t^M,\theta_y)]^2}. \quad \text{(A-14)}$$

Equation A-14 describes a diffraction time approximation relevant for a full 3D prestack time migration. We see that a 3D prestack time-migration velocity field is equivalent to the knowledge of the 2×2 symmetric matrix $\mathbf{M}^{(x)}(\bar{\mathbf{x}}^M,t^M)$ at each point $(\bar{\mathbf{x}}^M,t^M)$ of the time-migrated volume. In other words, the three independent elements of that matrix need to be known at each time-migrated point.

In the particular situation that the half-offset vector $\bar{\mathbf{y}}$ is always parallel to the aperture vector $\bar{\mathbf{a}}$, in which we can write $\theta = \theta_a = \theta_y$, equation A-14 is recast in the simple form

$$t^D(\bar{\mathbf{x}}^M,t^M,a,y,\theta)^2 = t^{M^2} + \frac{4(a^2+y^2)}{[v^M(\bar{\mathbf{x}}^M,t^M,\theta)]^2}. \quad \text{(A-15)}$$

The above equation provides the diffraction-time approximation relevant for 2D prestack time migration. In the zero-offset situation ($y = 0$), equations 2 and A-15 are equivalent.

APPENDIX B

COMPARISON WITH THE APPROACH OF CAMERON ET AL. (2007)

The time-to-depth conversion procedure presented in this paper is based on the knowledge of migration velocity, $v^M(\bar{\mathbf{x}}^M,t^M,\theta)$, corresponding to a single azimuth θ. Cameron et al. (2007) presented a different time-to-depth conversion approach, relying on the complete information of the variation of migration velocity with azimuth. This information is contained in the matrix $\mathbf{M}^{(x)}(\bar{\mathbf{x}}^M,t^M)$. When matrix $\mathbf{M}^{(x)}$ is known for all relevant locations in the domain $(\bar{\mathbf{x}}^M,t^M)$, one easily can obtain the inverse matrix

$$\mathbf{N}^{(x)} = \mathbf{M}^{(x)^{-1}}, \quad \text{(B-1)}$$

as well as the derivatives

$$\mathbf{W} = \frac{d\mathbf{N}^{(x)}}{dT} = 2\frac{d\mathbf{N}^{(x)}}{dt^M}. \quad \text{(B-2)}$$

Matrix $\mathbf{W}$, constituting the input data for the time-to-depth conversion in the approach of Cameron et al. (2007), is related to depth-domain velocity v and matrix $\mathbf{Q}_1^{(x)}$ by (see their equation 27)

$$\mathbf{W} = v^2(\mathbf{Q}_1^{(x)^T}\mathbf{Q}_1^{(x)})^{-1}. \quad \text{(B-3)}$$

Introducing a unit azimuth direction vector $\bar{\mathbf{u}}$ and using the above equation, one can write

$$v^2 = \bar{\mathbf{u}}^T\mathbf{W}\mathbf{E}\bar{\mathbf{u}}, \quad \text{(B-4)}$$

where matrix $\mathbf{E}$ is defined as

$$\mathbf{E} = \mathbf{Q}_1^{(x)^T}\mathbf{Q}_1^{(x)}. \quad \text{(B-5)}$$

Equation B-4 can be compared with our result

$$v^2 = (v_{\text{dix}}^M)^2F^2. \quad \text{(B-6)}$$

Equations B-4 and B-6 represent two bases for time-to-depth conversion and velocity estimation. The approach based on equation B-4, described by Cameron et al. (2007), uses as input matrix $\mathbf{W}$. The dynamic ray tracing required for calculation of matrix $\mathbf{E}$ involves calculation of matrices $\mathbf{Q}_1$ and $\mathbf{P}_1$, which means calculation of the second set of paraxial matrices is not required. The approach described in this paper, which is based on equation B-6, uses as input the time-migration interval velocity v_{dix}^M for a selected azimuth direction $\bar{\mathbf{u}}$. The dynamic ray-tracing procedure needed for calculation of factor F, however, requires calculation of both sets of paraxial matrices, $(\mathbf{Q}_I,\mathbf{P}_I)$.

APPENDIX C

VELOCITY SPREADING FACTOR FOR THE IMAGE RAY

Derivations for velocity spreading along the image ray in the 2D and multiazimuth 3D situations were given in Cameron et al. (2006, 2007). In this appendix, we derive equation 13 for the velocity spreading factor F pertaining to the single-azimuth 3D case. Our starting point is equation A-13, relating the azimuth-dependent migration velocity $v^M(\bar{\mathbf{x}}^M,t^M,\theta)$, to the 2×2 matrix, $\mathbf{M}^{(x)}(\bar{\mathbf{x}}^M,t^M)$, of second derivatives of one-way (upward) traveltime. Introducing the one-way, downward, migrated time $T = t^M/2$ and simplifying the notation, we can write

$$T[v^M]^2 = \frac{1}{\bar{\mathbf{u}}^T\mathbf{M}^{(x)}\bar{\mathbf{u}}}, \quad \text{(C-1)}$$

where $\bar{\mathbf{u}}$ is the direction vector for the migration azimuth used to obtain the migration velocity v^M. One can relate matrix $\mathbf{M}^{(x)}$ to the corresponding matrix $\mathbf{M}_2^{\uparrow}$ expressed in the ray-centered coordinates for the upward direction of the image ray, as follows,

$$\mathbf{M}^{(x)} = \mathbf{I}^*\mathbf{M}_2^{\uparrow}\mathbf{I}^*, \quad \text{(C-2)}$$

where

$$\mathbf{I}^* = \begin{pmatrix} -1 & 0 \\ 0 & 1 \end{pmatrix}. \quad \text{(C-3)}$$

Inserting $\mathbf{M}_2^{\downarrow} = \mathbf{P}_2^{\downarrow}\mathbf{Q}_2^{\downarrow^{-1}}$ and applying the relations for backward propagation of the ray propagator matrix in Iversen (2006), we obtain

$$\mathbf{M}^{(x)} = \mathbf{I}^*(\mathbf{I}^*\mathbf{Q}_1^T\mathbf{I}^*)(\mathbf{I}^*\mathbf{Q}_2^T\mathbf{I}^*)^{-1}\mathbf{I}^* = \mathbf{Q}_1^T\mathbf{Q}_2^{-T} = \mathbf{Q}_2^{-1}\mathbf{Q}_1. \tag{C-4}$$

The last operation is a consequence of the fact that matrix $\mathbf{M}^{(x)}$ is symmetric. Considering again equation C-1, the migration velocity therefore can be calculated from the equation

$$T[v^M]^2 = \frac{1}{\bar{\mathbf{u}}^T\mathbf{Q}_2^{-1}\mathbf{Q}_1\bar{\mathbf{u}}}. \tag{C-5}$$

Substituting equation C-5 into the Dix velocity equation 3, we obtain the important relation

$$(v_{\text{dix}}^M)^2 = \frac{d}{dT}\left[\frac{1}{\bar{\mathbf{u}}^T\mathbf{Q}_2^{-1}\mathbf{Q}_1\bar{\mathbf{u}}}\right] = -\frac{\bar{\mathbf{u}}^T\dfrac{d}{dt}[\mathbf{Q}_2^{-1}\mathbf{Q}_1]\bar{\mathbf{u}}}{[\bar{\mathbf{u}}^T\mathbf{Q}_2^{-1}\mathbf{Q}_1\bar{\mathbf{u}}]^2}. \tag{C-6}$$

To compute the derivative in the above equation, we observe that for an isotropic medium, the differential equation for paraxial matrix $\mathbf{Q}_I$, for $I = 1,2$, is

$$\frac{d\mathbf{Q}_I}{dT} = v^2\mathbf{P}_I \quad \text{and also} \quad \frac{d\mathbf{Q}_I^{-1}}{dT} = -v^2\mathbf{Q}_I^{-1}\mathbf{P}_I\mathbf{Q}_I^{-1}. \tag{C-7}$$

The rightmost equation was obtained under the application of the generic formula

$$\frac{d\mathbf{A}^{-1}}{dT} = -\mathbf{A}^{-1}\frac{d\mathbf{A}}{dT}\mathbf{A}^{-1}, \tag{C-8}$$

which results from differentiating both sides of the identity $\mathbf{A}^{-1}\mathbf{A} = \mathbf{I}$, followed by application of the leftmost equation C-7. Using the chain rule and taking into account equation C-7, we get

$$\begin{aligned}\frac{d}{dT}[\mathbf{Q}_2^{-1}\mathbf{Q}_1] &= v^2[-\mathbf{Q}_2^{-1}\mathbf{P}_2\mathbf{Q}_2^{-1}\mathbf{Q}_1 + \mathbf{Q}_2^{-1}\mathbf{P}_1] \\ &= -v^2\mathbf{Q}_2^{-1}[\mathbf{P}_2\mathbf{Q}_2^{-1} - \mathbf{P}_1\mathbf{Q}_1^{-1}]\mathbf{Q}_1 \\ &= -v^2\mathbf{Q}_2^{-1}\mathbf{Q}_2^{-T},\end{aligned} \tag{C-9}$$

where we have used the identity

$$\mathbf{P}_2\mathbf{Q}_2^{-1} - \mathbf{P}_1\mathbf{Q}_1^{-1} = \mathbf{Q}_2^{-T}\mathbf{Q}_1^{-1}, \tag{C-10}$$

which is a property of the ray-propagator matrix (see, for example, Červený, 2001, equation 4.3.16). Substitution into the Dix velocity formula C-6 yields

$$(v_{\text{dix}}^M)^2 = v^2\frac{\bar{\mathbf{u}}^T\mathbf{Q}_2^{-1}\mathbf{Q}_2^{-T}\bar{\mathbf{u}}}{[\bar{\mathbf{u}}^T\mathbf{Q}_2^{-1}\mathbf{Q}_1\bar{\mathbf{u}}]^2}. \tag{C-11}$$

from which

$$F^2 = \frac{v^2}{(v_{\text{dix}}^M)^2} = \frac{[\bar{\mathbf{u}}^T\mathbf{Q}_2^{-1}\mathbf{Q}_1\bar{\mathbf{u}}]^2}{\bar{\mathbf{u}}^T\mathbf{Q}_2^{-1}\mathbf{Q}_2^{-T}\bar{\mathbf{u}}}. \tag{C-12}$$

Extracting the square root from both sides yields equation 13, given in the main text.

APPENDIX D

RELATING THE DERIVATIVES OF VELOCITY IN RAY COORDINATES AND LOCAL CARTESIAN COORDINATES

As in the algorithm derived by Cameron et al. (2007), our scheme requires us to connect the derivatives of velocity in ray and local Cartesian coordinates. More specifically, we need relations between the derivatives of the velocity functions $v(\gamma_1,\gamma_2,\gamma_3)$ and $v(q_1,q_2,q_3)$. First-order derivatives in the two coordinate systems are connected by

$$\frac{\partial v}{\partial\gamma_i} = \frac{\partial q_k}{\partial\gamma_i}\frac{\partial v}{\partial q_k}. \tag{D-1}$$

Further differentiation yields

$$\frac{\partial^2 v}{\partial\gamma_i\partial\gamma_j} = \frac{\partial q_k}{\partial\gamma_i}\frac{\partial q_l}{\partial\gamma_j}\frac{\partial^2 v}{\partial q_k\partial q_l} + \frac{\partial^2 q_k}{\partial\gamma_i\partial\gamma_j}\frac{\partial v}{\partial q_k}. \tag{D-2}$$

We multiply both sides of equation D-2 by derivatives $(\partial\gamma_i/\partial q_n)$ and $(\partial\gamma_j/\partial q_m)$. The result is

$$\frac{\partial^2 v}{\partial q_n\partial q_m} = \frac{\partial\gamma_i}{\partial q_n}\frac{\partial\gamma_j}{\partial q_m}\left(\frac{\partial^2 v}{\partial\gamma_i\partial\gamma_j} - \frac{\partial^2 q_k}{\partial\gamma_i\partial\gamma_j}\frac{\partial v}{\partial q_k}\right). \tag{D-3}$$

The derivatives needed specifically for dynamic ray tracing are $\partial^2 v/\partial q_N\partial q_M$. Recognizing that $\partial\gamma_3/\partial q_N = 0$ and that $\partial v/\partial q_3 = v^{-1}\partial v/\partial T$, we obtain

$$\begin{aligned}\frac{\partial^2 v}{\partial q_N\partial q_M} = \frac{\partial\gamma_I}{\partial q_N}\frac{\partial\gamma_J}{\partial q_M}&\left(\frac{\partial^2 v}{\partial\gamma_I\partial\gamma_J} - \frac{\partial^2 q_K}{\partial\gamma_I\partial\gamma_J}\frac{\partial v}{\partial q_K}\right) \\ &- v^{-1}\frac{\partial\gamma_I}{\partial q_N}\frac{\partial\gamma_J}{\partial q_M}\frac{\partial^2 q_3}{\partial\gamma_I\partial\gamma_J}\frac{\partial v}{\partial T}.\end{aligned} \tag{D-4}$$

In a similar way as for velocity v, one can relate derivatives of traveltime T in ray coordinates and local Cartesian coordinates, as follows:

$$\frac{\partial T}{\partial\gamma_i} = \frac{\partial q_k}{\partial\gamma_i}\frac{\partial T}{\partial q_k}, \tag{D-5}$$

$$\begin{aligned}\frac{\partial^2 T}{\partial\gamma_i\partial\gamma_j} &= \frac{\partial q_k}{\partial\gamma_i}\frac{\partial q_l}{\partial\gamma_j}\frac{\partial^2 T}{\partial q_k\partial q_l} \\ &\quad + \frac{\partial^2 q_k}{\partial\gamma_i\partial\gamma_j}\frac{\partial T}{\partial q_k}.\end{aligned} \tag{D-6}$$

In the following, we consider only ray coordinates γ_I. Moreover, we recognize that traveltime T is constant along a wavefront, which means that $\partial T/\partial q_K = 0$ and $\partial^2 T/\partial\gamma_I\partial\gamma_J = 0$. Consequently, equation D-6 can be restated as

$$0 = \frac{\partial q_K}{\partial\gamma_I}\frac{\partial q_L}{\partial\gamma_J}\frac{\partial^2 T}{\partial q_K\partial q_L} + \frac{\partial^2 q_3}{\partial\gamma_I\partial\gamma_J}\frac{\partial T}{\partial q_3}. \tag{D-7}$$

Applying the definition $M_{KL} = \partial^2 T/\partial q_K\partial q_L$ and inserting $\partial T/\partial q_3 = v^{-1}$, we obtain

$$\frac{\partial^2 q_3}{\partial \gamma_I \partial \gamma_J} = -v\frac{\partial q_K}{\partial \gamma_I}\frac{\partial q_L}{\partial \gamma_J}M_{KL}. \quad \text{(D-8)}$$

The last result is substituted into equation D-4, which yields

$$\frac{\partial^2 v}{\partial q_N \partial q_M} = \frac{\partial \gamma_I}{\partial q_N}\frac{\partial \gamma_J}{\partial q_M}\left(\frac{\partial^2 v}{\partial \gamma_I \partial \gamma_J} - \frac{\partial^2 q_K}{\partial \gamma_I \partial \gamma_J}\frac{\partial v}{\partial q_K}\right) + M_{NM}\frac{\partial v}{\partial T}. \quad \text{(D-9)}$$

Therefore, for a situation in which the effect of the derivatives $\partial^2 q_K/\partial\gamma_I\partial\gamma_J$ is negligible, we can use in matrix form the approximation

$$\frac{\partial^2 v}{\partial \bar{\mathbf{q}}^2} = \mathbf{Q}_1^{-T}\frac{\partial^2 v}{\partial \bar{\boldsymbol{\gamma}}^2}\mathbf{Q}_1^{-1} + \mathbf{M}_1\frac{\partial v}{\partial T}, \quad \text{(D-10)}$$

where $\mathbf{M}_1 = \mathbf{P}_1\mathbf{Q}_1^{-1}$.

APPENDIX E

COMPUTATION OF VELOCITY DERIVATIVES ALONG THE IMAGE RAY

In this appendix, we describe an approach for computation of the first and second derivatives, $\partial v/\partial \boldsymbol{\gamma}$ and $\partial^2 v/\partial \boldsymbol{\gamma}^2$, at each ray coordinate vector $\boldsymbol{\gamma}$, that are required for our image-ray tracing scheme. Twice differentiation of equation 12 yields

$$\frac{\partial v}{\partial \gamma_i} = \frac{\partial v_{\text{dix}}^M}{\partial \gamma_i}F + v_{\text{dix}}^M\frac{\partial F}{\partial \gamma_i} \quad \text{(E-1)}$$

and

$$\frac{\partial^2 v}{\partial \gamma_i \partial \gamma_j} = \frac{\partial^2 v_{\text{dix}}^M}{\partial \gamma_i \partial \gamma_j}F + \left[\frac{\partial v_{\text{dix}}^M}{\partial \gamma_i}\frac{\partial F}{\partial \gamma_j} + \frac{\partial v_{\text{dix}}^M}{\partial \gamma_j}\frac{\partial F}{\partial \gamma_i}\right] + v_{\text{dix}}^M\frac{\partial^2 F}{\partial \gamma_i \partial \gamma_j}. \quad \text{(E-2)}$$

Because v_{dix}^M and its derivatives are known, our problem reduces to finding the derivatives of the velocity-spreading factor F, given by equation 13. The factor F depends on matrices $\mathbf{Q}_1$ and $\mathbf{Q}_2$ of the dynamic ray-tracing system. In view of the discussion related to equation 19, it is clear that for a time-to-depth-conversion procedure based on tracing single image rays, one has to make the approximation that the derivatives of factor F with respect to γ_I, along a given ray, are neglected. As a consequence, only the derivatives in equations E-1 and E-2 of F with respect to T survive.

One can show finally that our integration procedure does not rely on the second derivatives $\partial^2 v/\partial T^2$, which means calculation of the second derivative $\partial^2 F/\partial T^2$ is not required. Equations E-1 and E-2 therefore can be restated as

$$\frac{\partial v}{\partial \gamma_I} = \frac{\partial v_{\text{dix}}^M}{\partial \gamma_I}F, \quad \frac{\partial v}{\partial T} = \frac{\partial v_{\text{dix}}^M}{\partial T}F + v_{\text{dix}}^M\frac{\partial F}{\partial T}$$

and

$$\frac{\partial^2 v}{\partial \gamma_I \partial \gamma_J} = \frac{\partial^2 v_{\text{dix}}^M}{\partial \gamma_I \partial \gamma_J}F. \quad \text{(E-3)}$$

Given the above approximations, we are reduced thus to the calculation of $\partial F/\partial T$. For that matter, it is convenient to introduce the quantities

$$A = \bar{\mathbf{u}}^T\mathbf{Q}_2^{-1}\mathbf{Q}_1\bar{\mathbf{u}} \quad \text{and } B = \bar{\mathbf{u}}^T\mathbf{Q}_2^{-1}\mathbf{Q}_2^{-T}\bar{\mathbf{u}}, \quad \text{(E-4)}$$

from which we can write F and $\partial F/\partial T$ as (see equation 13)

$$F = \frac{A}{B^{1/2}} \quad \text{and} \quad \frac{\partial F}{\partial T} = \frac{\partial A}{\partial T}B^{1/2} - \frac{A}{2B^{3/2}}\frac{\partial B}{\partial T}. \quad \text{(E-5)}$$

It remains for us to obtain $\partial A/\partial T$ and $\partial B/\partial T$. Working similarly to the derivation of equation C-9, we readily find

$$\frac{\partial A}{\partial T} = -v^2\bar{\mathbf{u}}^T\mathbf{Q}_2^{-1}\mathbf{Q}_2^{-T}\bar{\mathbf{u}} = -v^2B$$

and

$$\frac{\partial B}{\partial T} = -2v^2\bar{\mathbf{u}}^T\mathbf{Q}_2^{-1}\mathbf{P}_2\mathbf{Q}_2^{-1}\mathbf{Q}_2^{-T}\bar{\mathbf{u}}. \quad \text{(E-6)}$$

It must be noted that the above formulas for factor F and its derivative $\partial F/\partial T$ cannot be used for zero migration time, for which $B = 0$. We find, however, that a second-order approximation for the factor F in the vicinity of $T = 0$ is given by

$$F = 1 - \frac{1}{2}vT^2\bar{\mathbf{u}}^T\frac{\partial^2 v}{\partial \bar{\boldsymbol{\gamma}}^2}\bar{\mathbf{u}}, \quad \text{(E-7)}$$

which yields, at $T = 0$,

$$F = 1, \quad \frac{\partial F}{\partial T} = 0. \quad \text{(E-8)}$$

In the 2D situation, we have

$$F = Q_1, \quad \frac{\partial F}{\partial T} = \frac{dQ_1}{dT} = v^2P_1, \quad \text{(E-9)}$$

which is reduced to equation E-8 in the limit of zero time because at that time, $Q_1 = 1$ and $P_1 = 0$.

REFERENCES

Black, J. L., and M. A. Brzostowski, 1994, Systematics of time-migration errors: Geophysics, **59**, 1419–1434.

Cameron, M. K., S. Fomel, and J. A. Sethian, 2006, Seismic velocity estimation and time to depth conversion of time-migrated images: 76th Annual International Meeting, SEG, Expanded Abstracts, 3066–3070.

———, 2007, Seismic velocity estimation from time migration: Inverse Problems, **23**, 1329–1369.

Červený, V., 2001, Seismic ray theory: Cambridge University Press.

Fomel, S., 2003, Time migration velocity analysis by velocity continuation: Geophysics, **68**, 1662–1672.

Hale, D., 1984, Dip-moveout by Fourier transform: Geophysics, **49**, 741–757.

Hubral, P., 1977, Time migration — Some ray theoretical aspects: Geophysi-

cal Prospecting, **25**, 738–745.
Hubral, P., and T. Krey, 1980, Interval velocities from seismic reflection time measurements: SEG.
Iversen, E., 2006, Amplitude, Fresnel zone, and NMO velocity for PP and SS normal-incidence reflections: Geophysics, **71**, no. 2, W1–W14.
Iversen, E., K. Åstebøl, and H. Gjøystdal, 1987, Time-to-depth conversion of 3D seismic interpretation data by use of "dynamic image ray": 49th Annual International Meeting, European Association of Exploration Geophysicists, Extended Abstracts, 16.
——–, 1988, 3D time-to-depth conversion of interpreted time-migrated horizons by use of the paraxial image ray method: Internal report, NORSAR, Norway.
Popov, M. M., and I. Pšenčík, 1978, Computation of ray amplitudes in inhomogeneous media with curved interfaces: Studia Geophysica et Geodaetica, **22**, 248–258.
Robein, E., 2003, Velocities, time-imaging and depth-imaging in reflection seismics: Principles and methods: EAGE.
Tygel, M., J. Schleicher, and P. Hubral, 1996, A unified approach to 3-D seismic reflection imaging, Part II: Theory: Geophysics, **61**, 759–775.
Whitcombe, D. N., 1994, Fast model building using demigration and single-step ray migration: Geophysics, **59**, 439–449.
Yilmaz, Ö., 2001, Seismic data analysis: Processing, inversion, and interpretation of seismic data, v. 1 and 2: SEG.